

UNIVERSITY OF SOUTHAMPTON
FACULTY OF PHYSICAL SCIENCES AND ENGINEERING
Department of Physics & Astronomy

Disc Winds Matter: Modelling Accretion and Outflow on All Scales

by
James Matthews

A thesis submitted for the degree of Doctor of Philosophy

May 2016

“Here, on the edge of what we know, in contact with the ocean of the unknown, shines the mystery and the beauty of the world.

And it’s breathtaking.”

Seven Brief Lessons on Physics, Carlo Rovelli

“Good enough for government work.”

Christian Knigge

UNIVERSITY OF SOUTHAMPTON

ABSTRACT

FACULTY OF PHYSICAL SCIENCES AND ENGINEERING

Department of Physics & Astronomy

Doctor of Philosophy

DISC WINDS MATTER: MODELLING ACCRETION AND OUTFLOW ON ALL SCALES

by James Matthews

Outflows are ubiquitous in accreting systems across 10 orders of magnitude in mass, and there is good evidence that mass-loaded winds are launched from the accretion discs of quasars and cataclysmic variables (CVs). Perhaps the most spectacular evidence for accretion disc winds is the blue-shifted, broad absorption lines (BALs) in UV resonance lines, seen in CVs and the BAL quasars. As well as imprinting absorption features, disc winds may affect the line and continuum emission from accreting objects. They thus offer a natural way to *unify* much of the phenomenology of CVs and active galactic nuclei (AGN).

In this thesis, I use a state-of-the-art Monte Carlo radiative transfer (MCRT) code, PYTHON, to conduct a series of simulations designed to test simple biconical disc wind models. I outline the MCRT techniques used, before describing a series of code validation exercises. Having tested my methods thoroughly, I explore whether the winds that are responsible for the UV BALs in high-state CVs could also have an effect on the optical spectrum. I find that the wind produces strong emission in the Balmer series, He II 4686 Å and a series of He I lines. The model shows the observed trends with inclination and in some cases produces sufficient recombination continuum emission to fill in the Balmer photoabsorption edge intrinsic to disc atmospheres. The results suggest that disc winds could have a significant impact on the optical spectra of high-state CVs.

The next step was to apply the techniques to quasar winds in a test of disc wind unification models. In previous efforts, the outflow tended to become ‘over-ionized’, and BAL features were only present if the X-ray luminosity was limited to around 10^{43} erg s $^{-1}$. The outflow also failed to produce significant line emission. Motivated by these problems, I introduce a simple treatment of clumping and find that it allows BAL features to form in the rest-frame UV at more realistic X-ray luminosities. The fiducial model shows good agreement with AGN X-ray properties and the wind produces strong line emission. Despite these successes, the model cannot reproduce all emission lines seen in quasar spectra with the correct equivalent width (EW) ratios, and I find the emission line EWs have a strong dependence on inclination.

Informed by the quasar wind modelling, I examine the emission line EW distributions of quasars in the context of geometric unification. I find that the observed distributions are not consistent with a model in which an equatorial BAL outflow rises from a foreshortened accretion disc. I discuss this finding in the context of other observational orientation indicators. Finally, I summarise my findings and suggest avenues for future work. Overall, the work presented here suggests that *disc winds matter*. They not only act as a spectral ‘filter’ for the underlying accretion continuum, but may actually dominate the emergent spectrum from accreting objects. As a result, unveiling their driving mechanisms, mass-loss rates and ionization structure is an important goal for the astronomical community.

Contents

Abstract	iv
List of Figures	ix
List of Tables	xi
Declaration of Authorship	xiii
Acknowledgements	xv
Abbreviations	xvii
Physical Constants	xix
1 Quasar Emission Lines as Probes of Orientation and Unification	1
1.1 Introduction	1
1.2 Data Sample	2
1.3 The Angular Distribution of Emission from an Accretion Disc	6
1.3.1 Standard Thin Disc Models	6
1.3.2 Including GR and Opacity Effects	7
1.4 Predicted EW Distributions Compared to Observations	7
1.4.1 Fitting the Quasar Distribution	7
1.4.2 Comparing non-BAL and LoBAL Distributions: Sample A	10
1.5 Discussion	14
1.5.1 Eigenvector 1	15
1.5.2 Polarisation	16
1.5.3 The Effect of Obscuration	19
1.5.4 Line Anisotropy	20
1.6 Conclusions	21
Bibliography	25

List of Figures

1.1	BH mass and Eddington fraction measurements for samples A and B.	3
1.2	Histograms of equivalent widths for three emission lines from the two different samples.	4
1.3	Angular variation of continuum luminosity from AGNSPEC and classical thin disc models.	8
1.4	Theoretical EW distributions from the numerical experiment described in section 1.4.1.	11
1.5	The EW[O III] distribution of quasars in the R11 sample and the best fit model.	12
1.6	χ^2/dof as a function of maximum angle.	13
1.7	The geometry of the toy model used to carry out the Monte Carlo simulations.	13
1.8	Heat map showing the results of the MC simulation described in section 1.4.2.	15
1.9	Eigenvector 1 for BAL and non-BAL quasars.	17
1.10	LoBAL fraction compared to mean LoBAL fraction in Eigenvector 1 space.	17
1.11	Histograms of polarisation percentages for BAL quasars from Schmidt et al. (1999) together with the Marin et al. (2014) AGN sample.	18
1.12	Cumulative distribution functions of the histograms shown in Fig. 1.11 for BAL quasars from Schmidt et al. (1999) together with the Marin et al. (2014) AGN sample. The colour-coding and x -axis scale are the same as Fig. 1.11. The translucent vertical lines mark the median value in each sample.	19

List of Tables

Declaration of Authorship

I, James Matthews, declare that this thesis titled, ‘Disc Winds Matter: Modelling Accretion and Outflow on All Scales’ and the work presented in it are my own. I confirm that:

- This work was done wholly or mainly while in candidature for a research degree at this University.
- Where any part of this thesis has previously been submitted for a degree or any other qualification at this University or any other institution, this has been clearly stated.
- Where I have consulted the published work of others, this is always clearly attributed.
- Where I have quoted from the work of others, the source is always given. With the exception of such quotations, this thesis is entirely my own work.
- I have acknowledged all main sources of help.
- Where the thesis is based on work done by myself jointly with others, I have made clear exactly what was done by others and what I have contributed myself.

The first two chapters of this thesis provide a general introduction to the field, and thus are based on the relevant literature. Where a figure is not produced by me, I have acknowledged this clearly with a credit to the relevant publication. Chapter 3 contains a description of the methods used. This is partly a description of the radiative transfer code PYTHON, which was originally developed by Knox Long and Christian Knigge ([Long & Knigge 2002](#)), but also includes substantial detail on the ‘macro-atom’ technique, which was proposed by Leon Lucy and incorporated into PYTHON by Stuart Sim for a study on young-stellar objects ([Sim et al. 2005](#)). Although I have put significant effort into testing, fixing and developing this scheme, I did not write the original code to deal with macro-atoms in PYTHON.

Chapter 4, 5 and 6 were studies I led under the guidance of my supervisor. For these chapters I conducted all simulations and data analysis, produced all the figures and wrote the text. A publication based on chapter 6 is in preparation, and chapters 4 and 5 are based on the following papers:

- Chapter 4: Matthews J. H., Knigge C., Long K. S., Sim S. A., Higginbottom N., ‘The impact of accretion disc winds on the optical spectra of cataclysmic variables’, 2015, MNRAS, 450, 3331.
- Chapter 5: Matthews J. H., Knigge C., Long K. S., Sim S. A., Higginbottom N., Mangham S. W., ‘Testing quasar unification: radiative transfer in clumpy winds’, 2016, MNRAS, 458, 293.

The following additional publications are not included in this thesis, although some of the work presented here did contribute towards the respective results

- Higginbottom N., Knigge C., Long K. S., Sim S. A., Matthews J. H., ‘A simple disc wind model for broad absorption line quasars’, 2013, MNRAS, 436, 2.3
- Higginbottom, N., Proga D., Knigge C., Long K. S., Matthews J. H., Sim S. A., ‘Line-driven Disk Winds in Active Galactic Nuclei: The Critical Importance of Ionization’ and Radiative Transfer, 2014, ApJ, 789, 1.
- Shankar F., Calderone G., Knigge C., Matthews J. H., et al., ‘The OpticalUV Emissivity of Quasars: Dependence on Black Hole Mass and Radio Loudness’, 2016, ApJ Letters, 818, 1.

Signed:

Date:

Acknowledgements

First and foremost, I would like to thank Christian Knigge, for being such an enthusiastic, helpful and stimulating supervisor throughout my PhD. Christian, I *always* left our meetings more positive than before – that speaks volumes – and I greatly enjoyed our conversations about science and Explosions in the Sky. I am also extremely grateful to Knox Long for all his assistance, writing the majority of the code and sharing some of his astronomy knowledge with me, and Stuart Sim for being immensely helpful throughout, especially when it comes to radiative transfer. I would also like to thank Nick Higginbottom for hours upon hours of assistance and friendship, and Sam Mangham for his help and input nearer the end of my PhD. To all of the above people; thank you for being part of a collaboration that does some great science, but also knew when to discuss a disastrous code bug with a knowing smile and ironic joke. I would also like to thank Daniel Proga, Omer Blaes, Ivan Hubeny, Shane Davis, Mike Brotherton, Mike DiPompeo, Frederic Marin, Daniel Capellupo, Dirk Grupe, Simo Scaringi, Adam Foster, Randall Smith, Chris Done, Anna Pala, Boris Gaensicke, Patrick Woudt and countless others for useful correspondence or stimulating scientific conversations. I am also very grateful to my masters supervisor Rosanne Di Stefano for inspiring me to continue doing research beyond my year in Boston.

Apart from those who I worked with, I am grateful to everyone who helped make Southampton a happy place to be over 3+ years. There are too many to name, but I will indulge a few. To my girlfriend Cat, thank you for being so patient with me and for so many lovely evenings. To Sam Connolly, you have been an ever-present and someone who I can always rely on for good beer, music and knowing looks. Sadie Jones, you were there when I needed you most for a cwtch or wanted to hear you pronounce year or ear. To Rob, Aarran, Juan, Georgios and Poppy, thanks for being true friends throughout the process. Big thanks to everyone else in the department for making it a super cool place to work, my office mates Mari, Judith, Stew and CFro, and my housemates Rich, Stu, Ollie, Sophie and Szymon. Thanks also goes to all the staff for being so friendly and approachable, particularly Poshak, Diego and Seb who have all helped me at various points through the PhD, and to Phil Charles for his sage advice since the early days.

There are also many people, outside of Southampton, who I must thank. Most of all, Mum, Dad, Beth and Nick, and the rest of my family. Thanks for supporting me

throughout my studies and just being all round lovely people. Thank you Josh, James and Alex, and our now manager John, for allowing me to play music that I love in Waking Aida. Eschaton and Full Heal were both released during my PhD, and in many ways they are each a thesis within themselves.

This work was supported by the Science and Technology Facilities Council via a 3.5 year PhD studentship. This work made use of the Sloan Digital Sky Survey. Funding for the Sloan Digital Sky Survey has been provided by the Alfred P. Sloan Foundation, the U.S. Department of Energy Office of Science, and the Participating Institutions. I acknowledge the use of the IRIDIS High Performance Computing Facility, and associated support services at the University of Southampton, in the completion of this work. Figures were produced using the `matplotlib` plotting library.

Abbreviations

AGN	Active galactic nuclei/nucleus
ADAF	Advection dominated accretion flow
BAL	Broad absorption line
BALQSO	Broad absorption line quasar
BBB	Big blue bump
BEL	Broad emission line
BH	Black hole
BI	Balnicity index
BL	Boundary Layer
BLR	Broad line region
CDF	Cumulative distribution function
CGS	Centimetre-gram-second
CV	Cataclysmic variable
DN(e)	Dwarf nova(e)
EW	Equivalent width
HERG	High excitation radio galaxy
HMXB	High-mass X-ray binary
HSE	Hydrostatic Equilibrium
IP	Intermediate polar
IR	Infra-red
ISCO	Innermost stable circular orbit
LHS	Left-hand side
LINER	Low ionization nuclear emission-line region
LMXB	Low-mass X-ray binary
LTE	Local thermodynamic equilibrium
MCRT	Monte Carlo radiative transfer

MRI	Magneto-Rotational Instability
NAL	Narrow absorption line
NEL	Narrow emission line
NLR	Narrow line region
NL	Nova-like variable
NS	Neutron Star
QSO	Quasa-stellar object / Quasar
RL	Radio-loud
RHS	Right-hand side
RIAF	Radiatively inefficient accretion flow
RLOF	Roche lobe overflow
SA	Sobolev approximation
SED	Spectral energy distribution
SFR	Star formation rate
sSFR	Specific star formation rate
SMBH	Supermassive black hole
SXSS	Soft X-ray excess
UFO	Ultra-fast outflow
UV	Ultraviolet
WA	Warm absorber
WD	White dwarf
WHIM	Warm, highly ionized medium
XRB	X-ray binary
YSO	Young stellar object

Physical Constants

Speed of light	$c = 2.997\ 924\ 58 \times 10^{10} \text{ cm s}^{-1}$
Boltzmann constant	$k = 1.380\ 658 \times 10^{-16} \text{ erg K}^{-1}$
Gravitational constant	$G = 6.672\ 599 \times 10^{-8} \text{ cm}^3 \text{ g}^{-1} \text{ s}^{-2}$
Solar mass	$M_{\odot} = 1.988\ 550 \times 10^{33} \text{ g}$
Solar radius	$L_{\odot} = 6.957\ 000 \times 10^{10} \text{ cm}$
Thomson cross-section	$\sigma_T = 6.652\ 458 \times 10^{-25} \text{ cm}^2$
Planck constant	$h = 6.626\ 076 \times 10^{-27} \text{ cm}^2 \text{ g s}^{-1}$
Stefan-Boltzmann constant	$\sigma = 5.670\ 367 \times 10^{-5} \text{ erg cm}^{-2} \text{ K}^{-4} \text{ s}^{-1}$
Parsec	$pc = 3.085\ 678 \times 10^{18} \text{ cm}$
Proton mass	$m_p = 1.672\ 621 \times 10^{-24} \text{ g}$
Electron mass	$m_e = 9.109\ 390 \times 10^{-28} \text{ g}$
Electron volt	$eV = 1.602\ 177 \times 10^{-12} \text{ erg}$
Electron charge	$q_e = 4.803\ 207 \times 10^{-10} \text{ esu}$
π	$= 3.141\ 593$
e	$= 2.718\ 282$

All constants are given to 6 decimal places, except for the speed of light which is exact. Throughout this thesis I use the centimetre-gram-second (CGS) system of units unless otherwise stated.

Dedicated to my family.

Chapter 1

Quasar Emission Lines as Probes of Orientation and Unification

This chapter is based on a paper in preparation:

Matthews J. H., Knigge C., ‘Quasar Emission Lines as Probes of Orientation and Unification’, to be submitted to MNRAS.

1.1 Introduction

In the previous chapter, I presented tests of geometric unification models using MCRT and photoionization simulations. One of the key results from that analysis is that trends with inclination prohibit models with equatorial outflows matching observations, as the EW of the emission lines tend to increase with inclination. This trend has clear implications for the geometries of BAL outflows; the viewing angle may determine many of the selection effects at work and must therefore be understood before the true covering factor of BAL outflows can be accurately determined. The covering factor and opening angle of the outflow are important quantities to measure in order to calculate the feedback efficiency (e.g. [Borguet et al. 2012](#)), and understand the outflow physics (e.g. [Proga 2005](#)).

Unlike in galactic accretion disc systems, measuring inclinations for quasars and AGN is notoriously difficult, and obtaining reliable orientation indicators is thus an important observational goal for the community. Perhaps as a result of this problem, directly

opposing geometries have been proposed for BAL outflows (see section ??). Here, I use observational data from the Sloan Digital Sky Survey to constrain the inclinations of BAL quasars. Similar attempts have been made previously with different diagnostics; for example, by considering radio measurements ([Zhou et al. 2006](#); [DiPompeo et al. 2012b](#)), polarisation ([Brotherton et al. 2006](#)) and emission line properties ([DiPompeo et al. 2012a](#)).

This chapter is structured as follows. First, I describe the data sample and selection criteria being used. I begin by simply examining the distributions of the EW of the [O III] 5007 Å emission line, EW[O III], and comparing the BAL and non-BAL quasar distributions. In section 1.3 I review the angular distribution of continuum emission one would expect from simple α -disc models, as well as exploring more advanced disc models computed with AGNSPEC. I then use these theoretical angular distributions applied to a simple toy model in section 1.4, and conduct MC simulations in an attempt to fit the observed LoBAL and non-BAL quasar distributions of EW[O III], using a similar approach to [Risaliti et al. \(2011\)](#). I also discuss the broad emission line distribution in HiBAL quasars more detail in this section. In section 1.5 I discuss the results in the context of radio and polarisation measurements of AGN, as well as exploring the location of BAL quasars in ‘Eigenvector 1’ parameter space. Finally, in section 1.6, I summarise the results.

1.2 Data Sample

The data sample is based upon the [Shen et al. \(2011\)](#), hereafter S11 catalog of 105,783 quasars from the The Sloan Digital Sky Survey (SDSS) Data Release 7 (DR7). As I will use emission line diagnostics in this study, this sample must be further divided according to which emission lines are present in the SDSS wavelength range at a given redshift. Sample A contains all quasars within the redshift range $0.35 < z < 0.83$, such that the Mg II 2800 Å and [O III] 5007 Å line EWs are both measured, and Mg II BAL identification is possible. Sample B contains all quasars within the redshift range $1.45 < z < 2.28$, such that the EWs and presence of BAL in Mg II 2800 Å and C IV 1550 Å are both measurable. The details of these samples are shown in table 1. The mass and Eddington fraction measurements from S11 of the two samples, are shown in Fig. 1.1 against the background distribution of all S11 quasars.

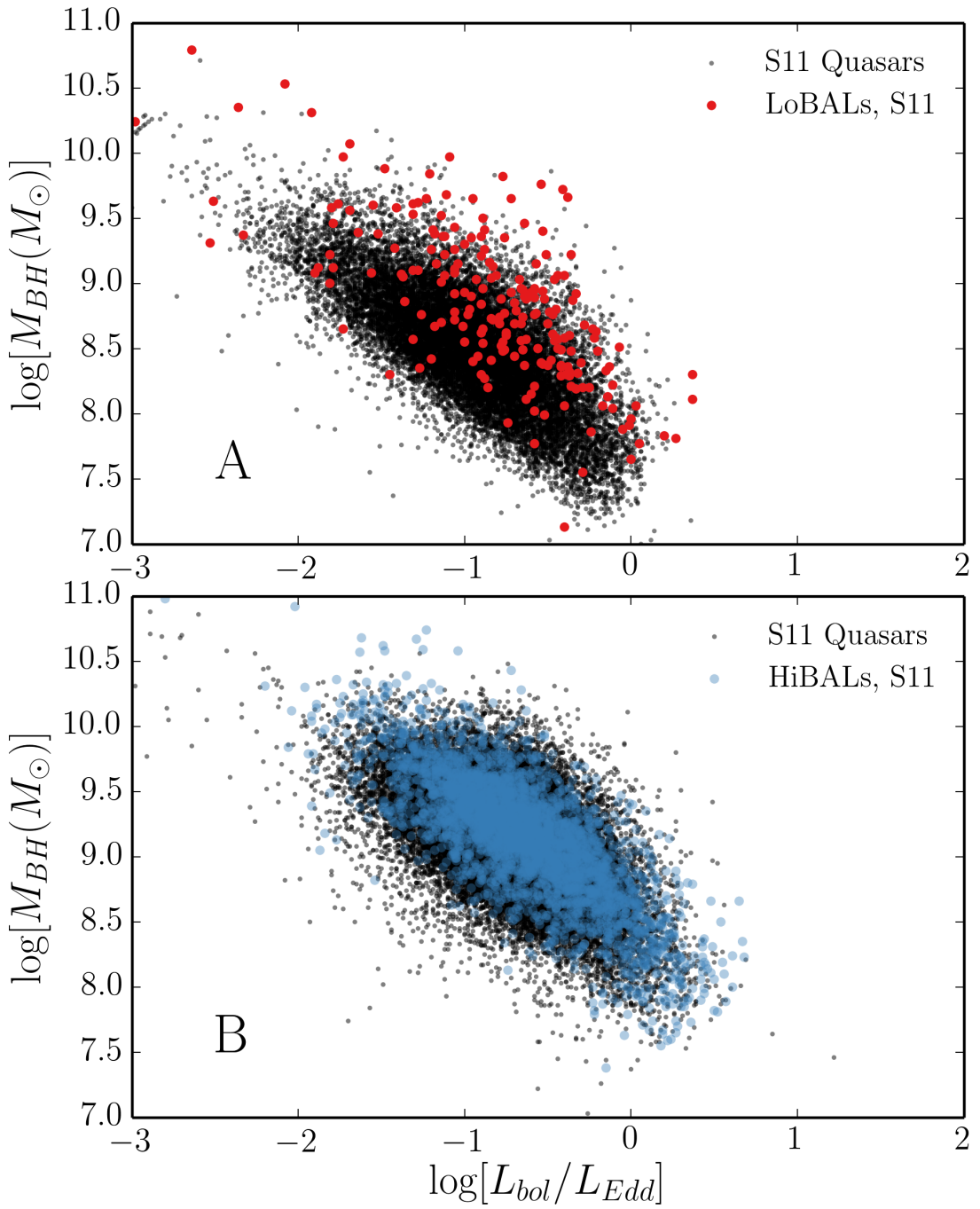


FIGURE 1.1: BH mass and Eddington fraction measurements from S11 for Sample A (top) and Sample B (bottom). The LoBALs in sample A and BALs in Sample B are also plotted in each case.

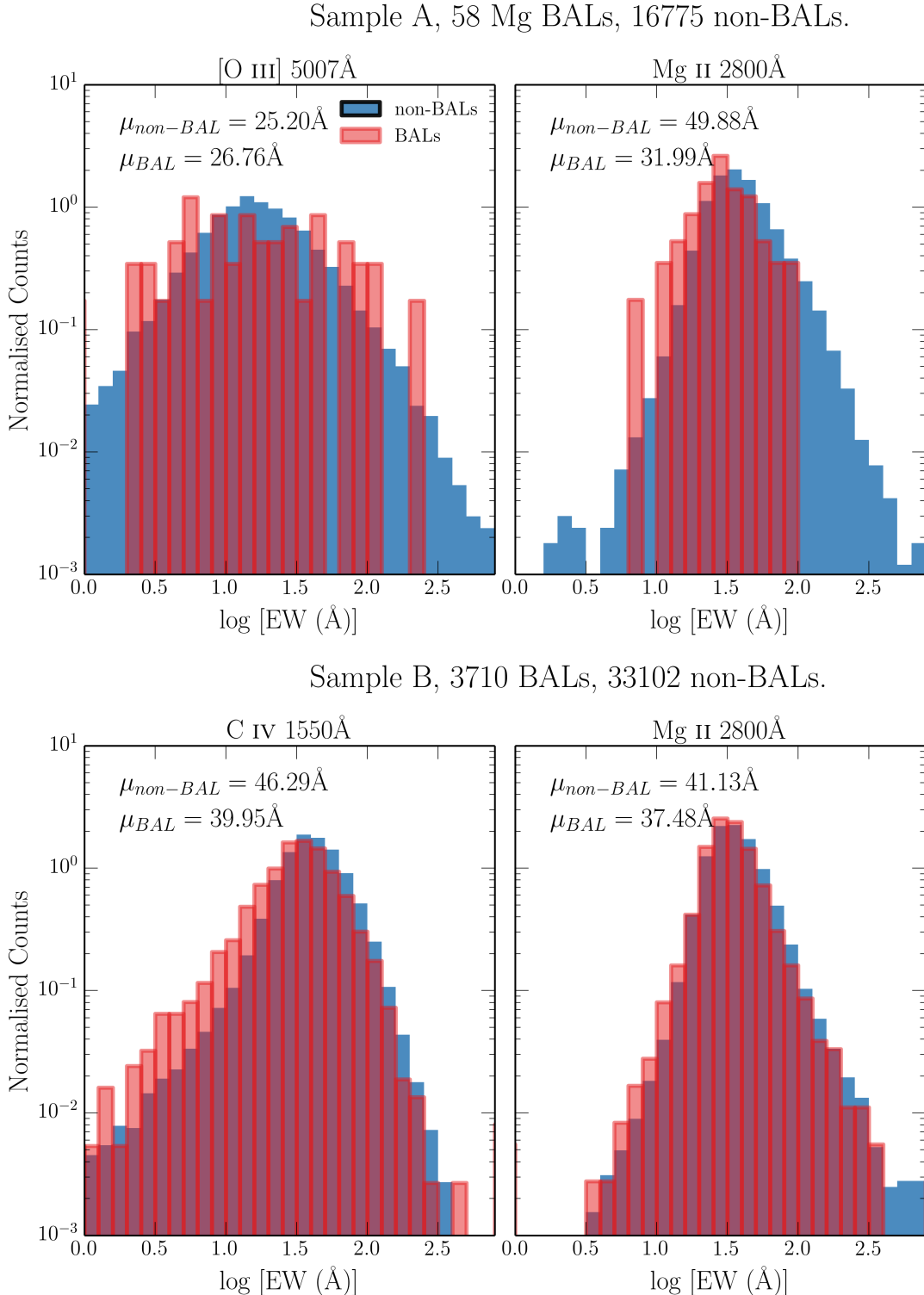


FIGURE 1.2: Histograms of equivalent widths for three emission lines from the two different samples. The mean of the BAL and non-BAL quasar distributions are labeled in each case, and the histograms are normalised so that they integrate to 1.

S11 are careful to take into account traditional problems with quasar line fitting, such as narrow line or Fe pseudocontinuum contamination, in their fits to emission line profiles and resultant EW measurements. For Mg II 2800 Å this includes careful subtraction of the Fe emission using the [Vestergaard & Wilkes \(2001\)](#) templates. This subtraction is not included for C IV 1550 Å, as the Fe emission is less prominent and harder to model. This may lead to a systematic overestimate by ~ 0.05 dex in the C IV line EW. The [O III] 5007 Å line is fitted with a Gaussian. The flux ratio of this line with the sister component of the doublet, [O III] 4959 Å, is found to agree well with the theoretical expectation of around 3, implying a reliable subtraction of broad H β . In order to mask out the effects of e.g., absorption, on the C IV and Mg II lines, S11 ignore 3σ outliers in the fit to the profile. Based on these considerations, the S11 catalog makes for a reliable set of EW measurements. This is especially true when making inferences from multiple emission lines, as systematics inherent to individual lines or spectral windows are less likely to affect the analysis as a whole.

In attempting to draw broad conclusions about unification models as a whole, I would ideally construct a large, homogenous dataset of *HiBAL* and non-BAL quasars, both with [O III] 5007 Å EWs. Unfortunately, the wavelength limits of SDSS do not allow this, and only LoBAL quasars have both BALs and EW[O III] measurements. One of the problems with using just LoBAL quasars in tests of unification is that there is evidence that they are drawn from a different population than normal quasars. Examples include anomalously high LoBAL fractions in dust-reddened quasar samples ([Urrutia et al. 2009](#)) and infra-red selected samples ([Dai et al. 2012](#)); although see also [Lazarova et al. \(2012\)](#).

Fig. 2 shows histograms of a number of different emission line properties for samples A and B. As discussed by previous authors (e.g. [Weymann et al. 1991](#)), I find that BAL and non-BAL quasars seem to possess very similar emission line properties. The EW is related to the intrinsic, ‘face-on’ equivalent width, EW_* by the equation

$$\text{EW} = \text{EW}_*/\epsilon(\theta) \quad (1.1)$$

where θ is the viewing angle with respect to the symmetry axis and $\epsilon(\theta)$ is the ‘angular emissivity function’, which describes how the continuum luminosity from the disc varies as a function of viewing angle. For a foreshortened disc this is simply $\epsilon(\theta) = \cos \theta$. Note that this assumes isotropic line emission, but the effect of line anisotropy is discussed in section [1.5.4](#).

Thus, if BALQSOs are preferentially viewed from larger-than-average viewing angles, we would expect them to possess higher EWs. We might also expect that the distribution of EWs is broader in this case due to the shape of a $\cos \theta$ curve. It is already apparent from Fig. 1.2 that the BALQSO distribution means are not significantly higher than the non-BAL quasar means – in fact, in many cases they are lower. This is not expected from a model in which the continuum comes from a foreshortened disc, and BAL outflows are at all equatorial. This problem is examined further in section 1.4. First, I will examine the motivations for different forms of $\epsilon(\theta)$ in AGN and quasars.

1.3 The Angular Distribution of Emission from an Accretion Disc

As introduced in chapter 1, the most widely-used theoretical model for accretion discs is the so-called ‘ α -disc’ model of SS73. There are a number of well-documented problems when fitting AGN SEDs with SS73 accretion disc models (see section ??), Despite these problems, Capellupo et al. (2015) succeeded fitting α -disc models to AGN spectra when the effects of GR, mass-loss and comptonisation were included. In this section, I start by discussing the angular distribution of emission from a classic SS73 disc, before exploring opacity and GR effects. In order to do so, I use AGNSPEC (Hubeny et al. 2000; Davis & Hubeny 2006; Davis et al. 2007). I stress that the discussion here is not limited to α -discs; the only real condition for the angular distributions derived here is that the disc is geometrically thin and optically thick.

1.3.1 Standard Thin Disc Models

Any geometrically thin, optically thick disc will appear foreshortened and limb darkened (if temperature decreases with height from the central disc plane). Foreshortening is a simple $\cos \theta$ geometric effect, where θ is the inclination with respect to the vertical z axis, which is perpendicular to the disc plane. Limb darkening, $\eta(\theta)$, is usually approximated by a linear dependence of the emergent flux on $\cos \theta$, i.e.

$$\eta(\theta) = a(1 + b \cos \theta), \quad (1.2)$$

where a is a normalisation constant, and b governs the strength of the limb darkening. Setting $b = 3/2$, known as the Eddington approximation, tends to give good agreement with solar observations (e.g. [Mihalas 1978](#)). The two effects can be combined to give a net angular emissivity function of

$$\epsilon(\theta) = a \cos \theta \left(1 + \frac{3}{2} \cos \theta \right). \quad (1.3)$$

1.3.2 Including GR and Opacity Effects

In reality, limb darkening is not frequency independent and depends on the bound-free and bound-bound opacities in the disc. In addition, it has been shown that GR light bending can ‘isotropize’ the radiation field in XRBs ([Zhang et al. 1997](#); [Muñoz-Darias et al. 2013](#)), in some cases overcoming foreshortening effects. In order to assess the impact of GR and disc opacities on $\epsilon(\theta)$, I use AGNSPEC models, which conducts a stellar atmosphere calculation to obtain the SED from a series of annuli, before using the KERRTRANS code to calculate the emergent SED by ray-tracing along Kerr geodesics. Fig. 1.3 shows $\epsilon(\theta)$ as a function of θ for two AGNSPEC models for minimally and maximally spinning BHs. The models are characterised by $M_{BH} = 10^9 M_\odot$ and an Eddington fraction of 0.2. The angular distribution is fairly insensitive to these choices. For comparison, I also show foreshortened and limb-darkened predictions for SS73 models. Although the AGNSPEC continua are significantly more isotropic at 500 Å, there is very little effect redward of around 1000 Å, which is the relevant region of $\epsilon(\theta)$ for [O III] 5007 Å, C IV 1550 Å and Mg II 2800 Å. In fact, using the foreshortened estimate is the conservative (least anisotropic) prescription in these regimes. I will thus adopt $\epsilon(\theta) = \cos \theta$ for the remainder of this work.

1.4 Predicted EW Distributions Compared to Observations

1.4.1 Fitting the Quasar Distribution

[Risaliti et al. \(2011\)](#), hereafter R11) analysed the EW[O III] distribution of 6029 quasars in SDSS DR5. They demonstrated that a foreshortened disc and isotropic [O III] 5007 Å line produces a high EW tail in the EW distribution, with a characteristic slope of

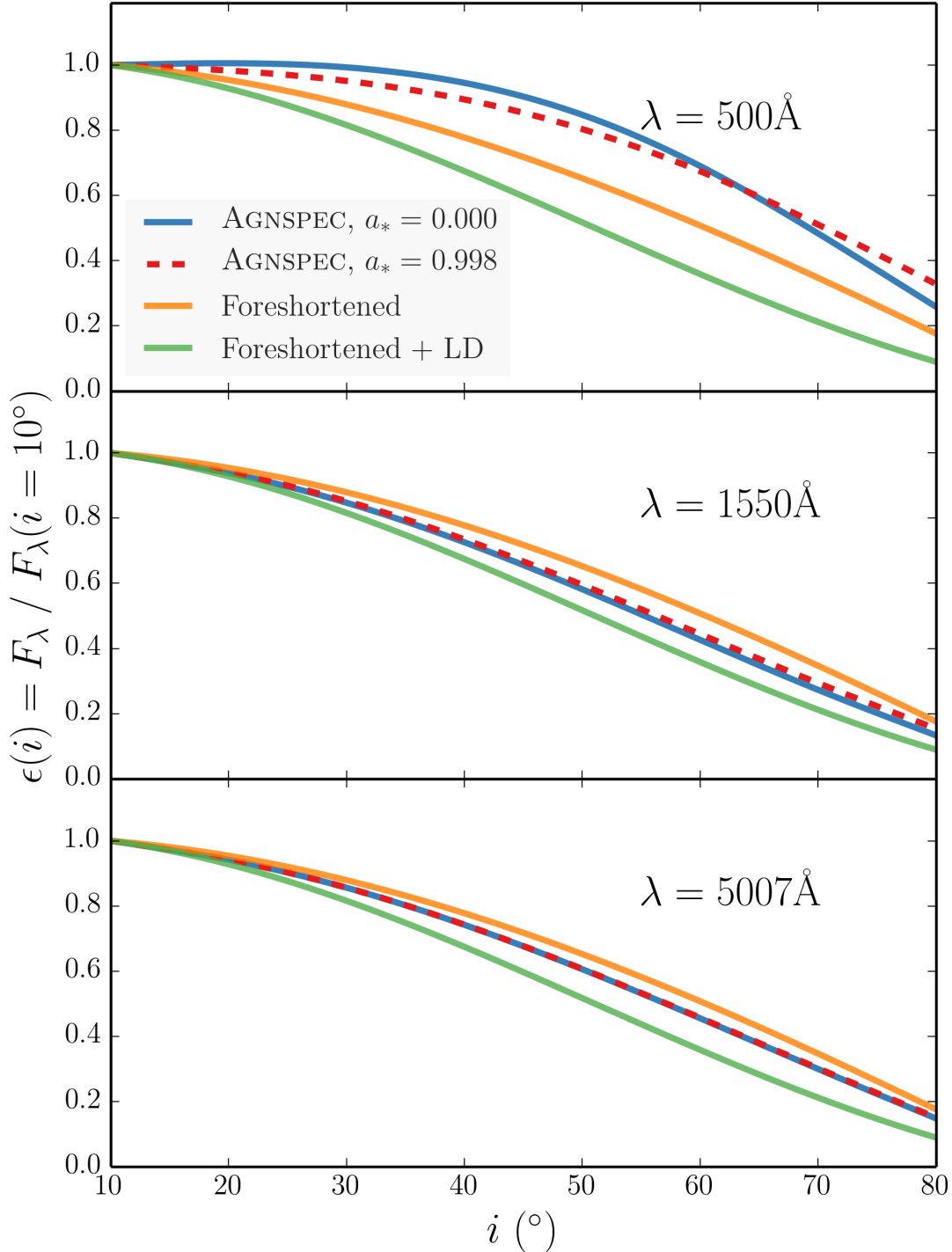


FIGURE 1.3: Angular variation of continuum luminosity from AGNSPEC and classical thin disc models. The monochromatic continuum luminosities is divided by the monochromatic continuum luminosity at 10° , from AGNSPEC and classical thin disc models, at three different wavelengths. The models are computed for an Eddington fraction of 0.2 and $M_{BH} = 10^9 M_\odot$. In each panel I show both Kerr and Schwarzschild AGNSPEC models, and the classical models are for both pure foreshortened discs and foreshortened and limb darkened (LD) discs.

$\Gamma_{EW} = -3.5$. In order to first reproduce their result and discuss its implications, I have created a sample according to their selection criteria. The criteria are that the object in question lies in the redshift range 0.01 to 0.8, have an absolute magnitude $M_i > 22$, an apparent magnitude $m_i > 19.1$, and signal to noise per pixel of greater than 5. Using the updated SDSS quasar sample of S11, this defines a sample of 14,424 quasars.

To fit the distribution, I conduct the following procedure, which is similar to the method R11 use to demonstrate that the power law tail is expected.

1. A set of isotropic angles is chosen such that $P(\theta) \propto d\Omega(\theta)$. If $\theta < \theta_1$ then the fake object is designated as unobscured, and otherwise the object is ignored.
2. To be included in the sample, the object also has to survive a selection test to simulate the distribution of angles in a flux-limited sample. This is done by drawing a random sample from the real quasar sample, and calculating a ‘doubly observed continuum flux’, F_O at 5100Å (rest frame), such that $F_O = F_{5100} \epsilon(\theta)$. The flux limit is set at 5×10^{-13} erg s⁻¹ cm⁻¹ Å⁻¹, but the results are fairly insensitive to the limit chosen.
3. For each mock sample, an EW_* is drawn from an intrinsic (i.e. ‘face-on’) EW distribution for quasars. This is assumed to be a Gaussian distribution. The mean, μ_* , and width, σ_* , of this Gaussian can either be set arbitrarily – for example, to demonstrate trends in mock data – or obtained from a χ^2 fit to the observed EW distribution.
4. A mock EW is estimated such that $EW = EW_*/\epsilon(\theta)$, and this process is repeated to build up a mock sample of 10^6 objects.

The result of this numerical experiment is, as found by R11, a distribution with a high EW tail of slope -3.5 . I can now vary the maximum angle, θ_1 , and examine how this tail changes. Mock data for a series of maximum angles is shown in Fig. 1.4, for two different intrinsic Gaussians. The power law behaviour is only seen when the maximum angle is sufficiently large, and a rapid decay in the distribution is observed at a characteristic EW related to both the width and mean of the intrinsic distribution as well as the cosine of the maximum angle. The top panel has μ_* and σ_* of the R11 Model 1, whereas the bottom panel shows a narrower distribution to illustrate the earlier onset of the high

EW cutoff. In principle, this cutoff could be used to infer information about the viewing angle distribution of quasars.

Fig. 1.5 shows the result of a χ^2 minimization fit to the R11 sample. The best fit is achieved with a maximum angle of $\theta_1 = 84^\circ$ and a narrower intrinsic distribution than model 1 of R11. The run of reduced χ^2 with maximum angle is shown in Fig. 1.6, where the choice for μ_* and σ_* is left free in each case. Maximum angles below $\sim 80^\circ$ are strongly disfavoured by this model. I adopt linear binning to facilitate easy comparison with R11, and only fit up $\text{EW} = 100\text{\AA}$ due to poor statistics above that limit. This makes inferring any information about a potential high EW cutoff difficult as a more complete sample at high EW is required.

1.4.2 Comparing non-BAL and LoBAL Distributions: Sample A

In order to compare the observed distributions to those expected for LoBALS and non-BALs I conduct a Monte Carlo simulation similar to the process described in section 1.4.1, but with a few key differences. I once again assume $\epsilon(\theta) = \cos \theta$. The geometry of the toy model used in this simulation is shown in Fig. 1.7.

First, A set of isotropic angles is generated. If $\theta_{min} < \theta < \theta_{max}$ then the fake object is flagged as a mock BAL. If $\theta < \theta_{min}$ then the fake object is designated a non-BAL, and otherwise the object is ignored. Once again, the object also has to survive a selection test based on a arbitrary flux selection limit. I then fit the non-BAL distribution using the method described previously. For each mock sample, a EW_* is drawn from the intrinsic gaussian, and a mock EW is estimated such that $\text{EW} = \text{EW}_*/\epsilon(\theta)$. This process is repeated to build up a mock sample of objects, and carried out for a series of pairs of θ_{min} and θ_{max} . This allows theoretical distributions for BAL and non-BAL quasars for a series of different outflow geometries to be derived.

The diagnostics recorded from the simulation are the following four quantities:

- The p -value associated with a two-tailed Kolgomorov-Smirnov (K-S) test statistic, p_{KS} , in which the mock BAL sample is compared to the real LoBAL sample.
- The BAL fraction, f_{BAL} , is calculated from the number of objects in the mock sample with $\theta_{min} < \theta < \theta_{max}$.

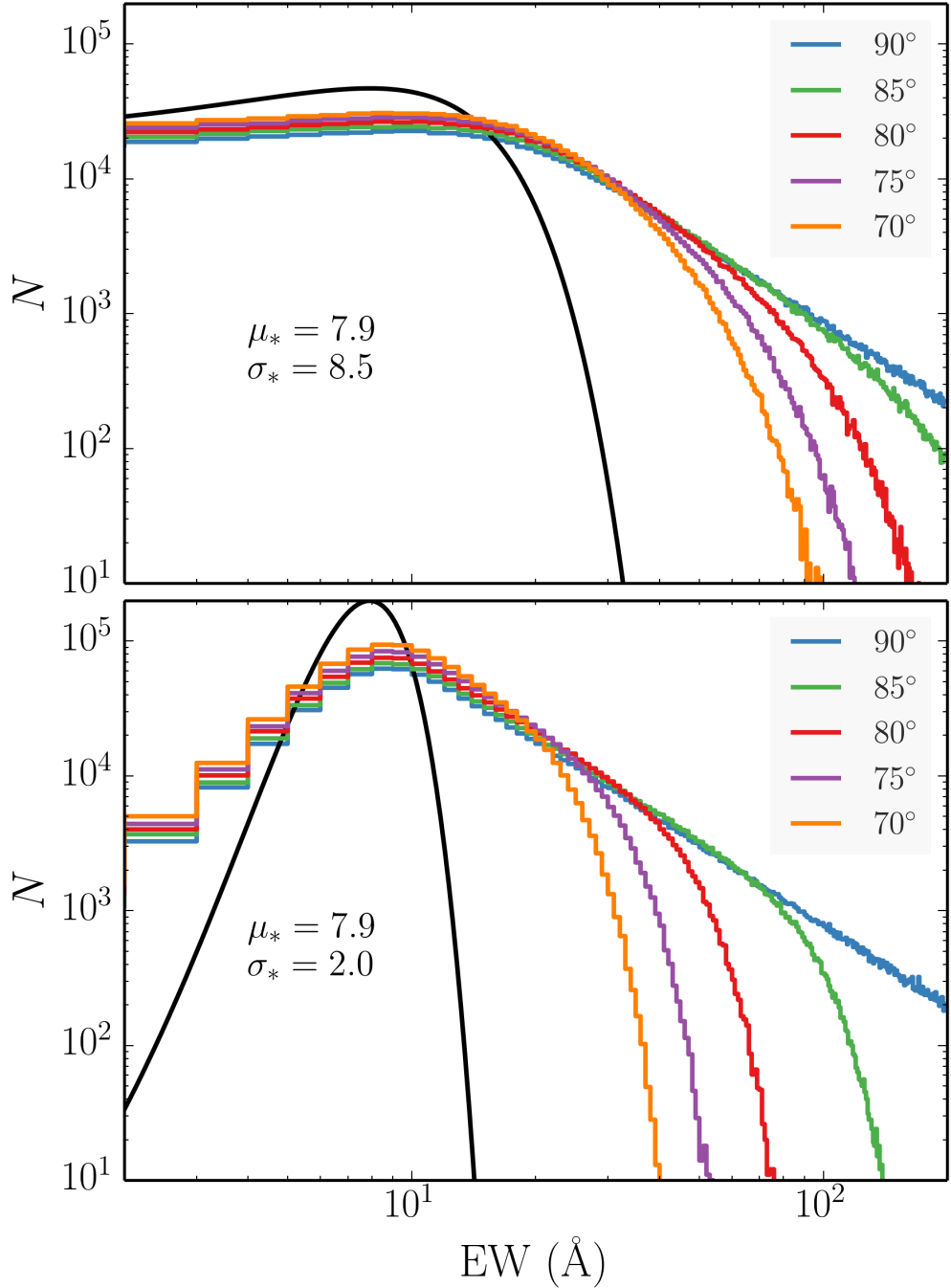


FIGURE 1.4: Theoretical EW distributions from the numerical experiment described in section 1.4.1 for a few different maximum angles. The results in the top panel use the same intrinsic distribution as Model 1 from R11 (shown in black), whereas the bottom panel shows the distributions obtained from a narrower intrinsic Gaussian. By the time the maximum angle is limited to around 70° the cutoff is clear even at moderate values of EW.

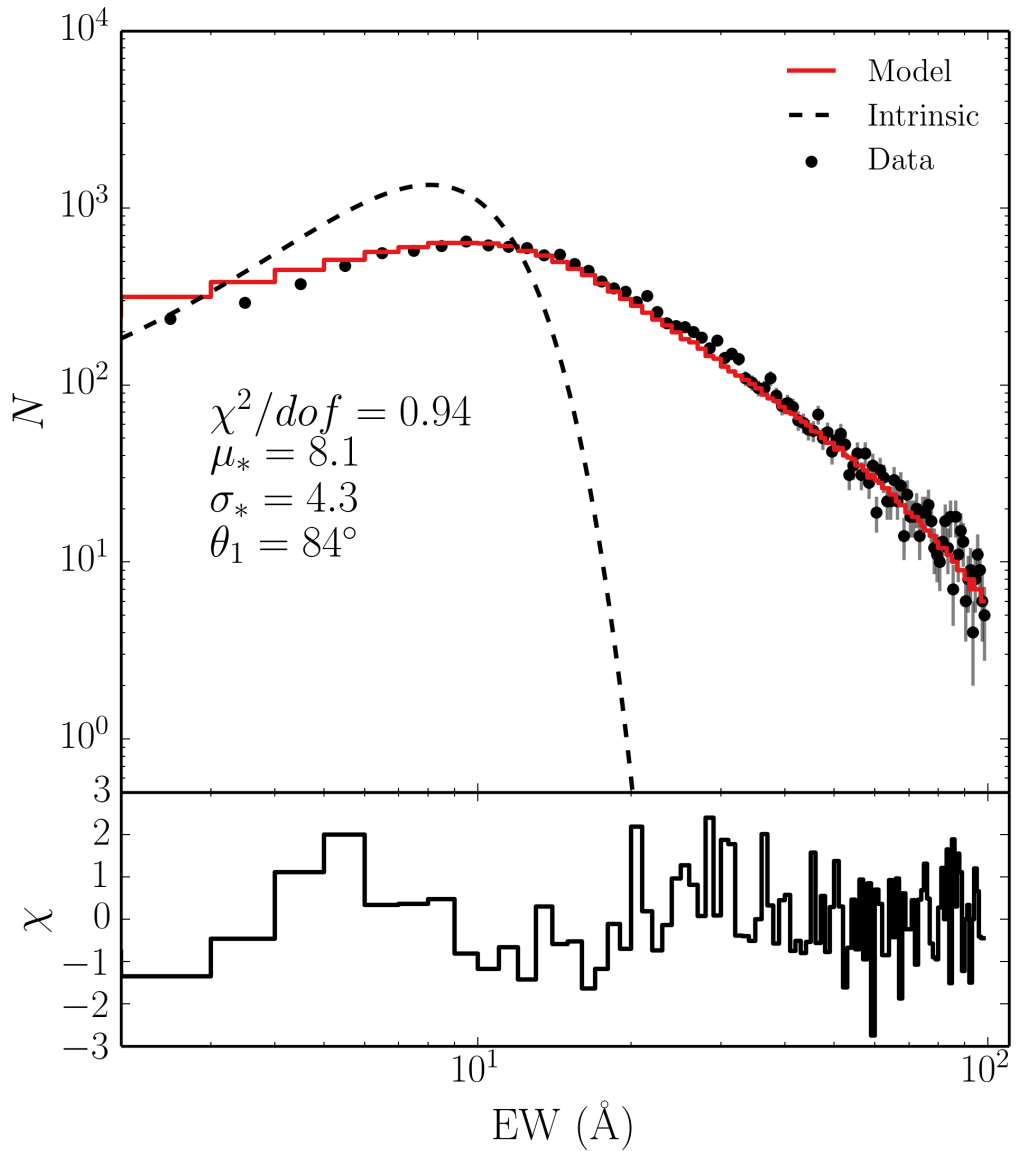


FIGURE 1.5: The $\text{EW}[\text{O III}]$ distribution of quasars in the R11 sample (black points), with \sqrt{N} errorbars, and the best fit model with a maximum viewing angle of 84° . The intrinsic Gaussian distribution is shown with a dotted line. The non-BAL plot is equivalent to the non-BAL histogram in the top left panel of Fig. 1.2, except that it uses linear binning and adopts the R11 sample criteria rather than using sample A.

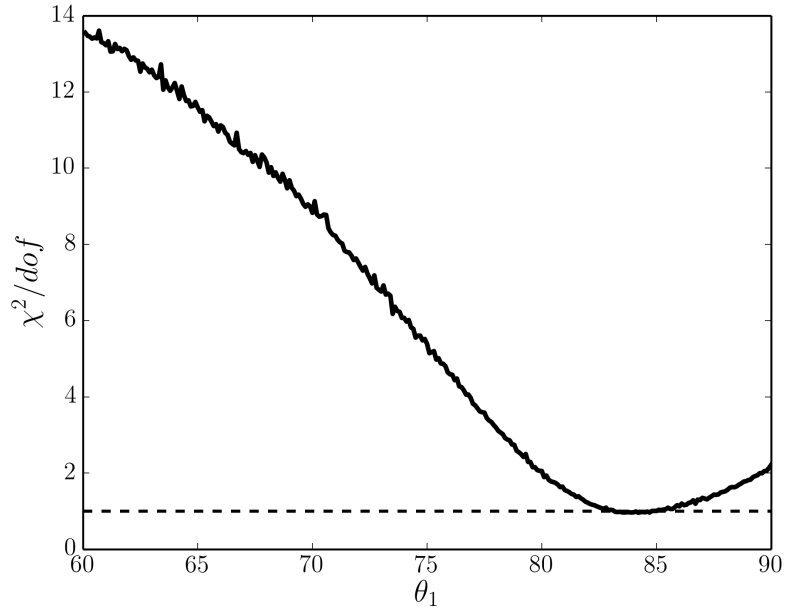


FIGURE 1.6: χ^2/dof as a function of maximum angle, θ_1 , calculated in steps of 0.1° .
The choice for μ_* and σ_* is left free in each case.

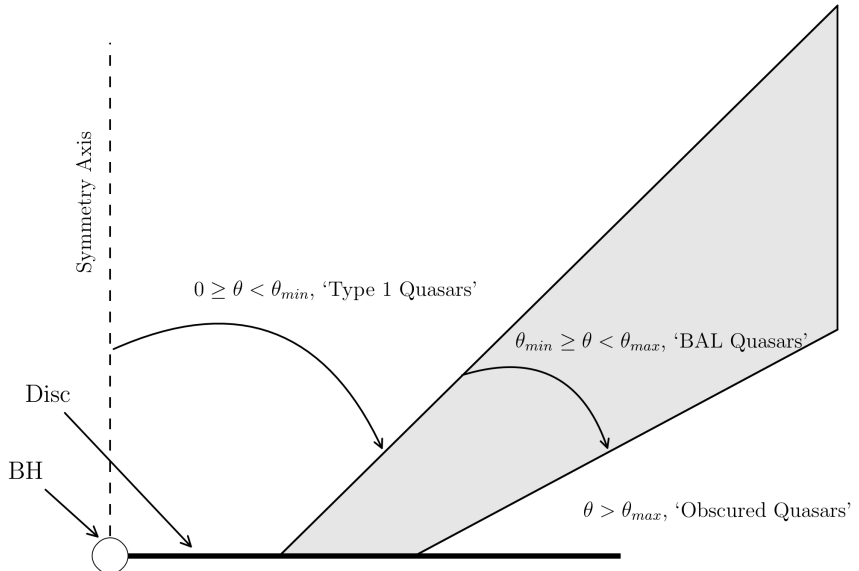


FIGURE 1.7: The geometry of the toy model used to carry out the Monte Carlo simulations.

- The χ^2/dof from the fit to the non-BAL quasar distribution.
- $\Delta\mu_{EW}$, the difference between the mean value of the mock BAL distribution and the mean value of the mock non-BAL distribution.

The simulation results are shown in figure 1.8, in which the four diagnostics are plotted as a function of θ_{min} and θ_{max} .

As expected, equatorial viewing angles for LoBAL quasars are disfavoured, and furthermore, it is only possible to fit the tail to the EW[O III] distribution if non-BAL quasars are allowed to be viewed from high inclinations. There is no region of parameter space where a satisfactory fit is obtained to the quasar distribution without simultaneously obtaining a large value of $\Delta\mu_{EW}$. The K-S test allows us to reject the null hypothesis. The simulations favour a geometry in which BAL quasars are viewed from very similar angles to non-BAL quasars.

The conclusions here are limited by the lack of knowledge about the intrinsic face-on distribution of EW[O III], or equivalently, the orientations of the quasars themselves. If either of these quantities were known then the results of the K-S test and χ^2 minimization could be used to place more robust constraints on BAL and non-BAL viewing angles and the associated covering factor of the outflow. Furthermore, the distribution of C IV quasar EW cannot be fit by the same model as the EW[O III] distribution.

A key limitation is due to the SDSS wavelength coverage and means that only LoBALS can be used when EW[O III] is present (sample A). I would suggest that future observational programs might look to build up a large sample of EW[O III] measurements for HiBAL quasars.

1.5 Discussion

I have demonstrated that the EW distributions of the [O III] 5007 Å emission line in LoBAL and non-BAL quasars is not consistent with a model in which LoBAL quasars are viewed from equatorial angles and the continuum emission originates from a foreshortened accretion disc. The EW distributions of C IV 1550 Å suggest that a similar conclusion applies to HiBAL quasars. This result would only be strengthened were I to include limb darkening. I will now explore how the above results compare to other

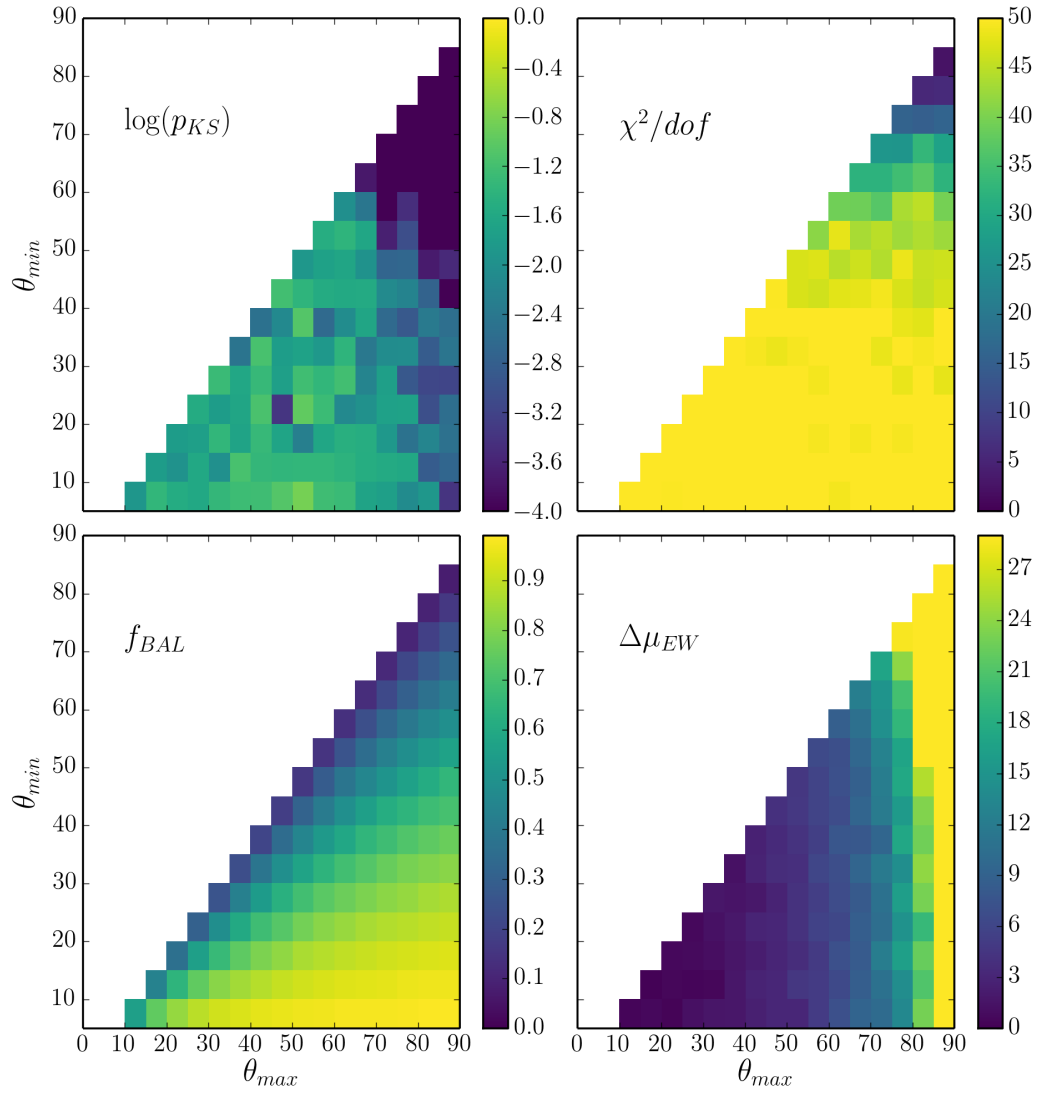


FIGURE 1.8: Heat map showing the results of the MC simulation described in section 1.4.2. The quantities shown are discussed further in the text, but correspond to (clockwise from top left): the p_{KS} value from a comparison between the mock BAL dataset and the observed BAL dataset, the reduced χ^2 from the fit to the non-BAL EW distribution, the difference in mean EW between the mock BAL and mock non-BAL datasets, and the BAL fraction expected for the geometry in question.

observations of quasars that might probe system orientation, as well as the potential impact of obscuration and line anisotropy on the results.

1.5.1 Eigenvector 1

Eigenvector 1 (EV1) is a fundamental parameter space for AGN and quasars (Boroson & Green 1992; Sulentic et al. 2000; Marziani et al. 2001; Shen & Ho 2014). It relates the FWHM of H β , the relative iron strength, R_{FeII} , and EW[O III]. Both EW[O III] and FWHM[H β] have been used as orientation indicators, and so comparing the LoBALQSO

EV1 distribution to the non-BAL quasar EV1 distribution is particularly interesting. Once again, HiBALs cannot be placed on this space due to the lack of rest-frame optical coverage.

Fig. 1.9 shows the quasar distribution from sample A in EV1 parameter space, with LoBAL quasars from sample A overplotted. [Shen & Ho \(2014\)](#), hereafter SH14) propose that the main inclination driver in this parameter space is FWHM[H β], and that high inclination sources should thus cluster around a diagonal line from the lower right to upper left quadrants. In contrast, R11’s analysis predicts that high inclination sources should cluster around high EW OIII widths. As EW[O III] and FWHM[H β] are very weakly correlated (Spearman’s rank coefficient of 0.14), this means they should lie to the left of the parameter space. Inspection of the figure clearly shows that BAL quasars are not only found in one region of the EV1 parameter space.

In order to assess this more quantitatively, I also show contours of quasar counts overlaid on the scatter plot. The contours correspond to the number of objects in each bin, where the bins are of size $\Delta R_{\text{FeII}} = 0.2$ and $\Delta \text{FWHM}[\text{H}\beta] = 500 \text{ km s}^{-1}$. The percentage of quasars falling within the inner contour is 45%, whereas only 18% of LoBALQSOs fall in the space. Conversely, 24% of LoBALQSOs fall outside the outermost contour compared to 10% of non-BAL quasars. It would therefore appear that BAL quasars are preferentially clustered towards the high-mass and high-inclination end of EV1 space (under the interpretation of SH14). This is further illustrated by Fig. 1.10, which shows the LoBAL fraction in larger bins, compared to the mean LoBAL fraction. This is again suggestive of an overdensity of LoBALQSOs towards the upper right of the parameter space. It is also clear that a unification picture in which BAL quasars are viewed exclusively from high inclinations is inconsistent both the R11 and SH14 interpretations.

Larger datasets, preferably including HiBAL quasars with EV1 measurements, are needed in order to properly constrain the EV1 behaviour of BAL quasars. However, overall, the behaviour of EV1 in LoBALQSOs slightly strengthens the conclusion that BAL quasars are not always viewed from extreme inclinations.

1.5.2 Polarisation

Spectropolarimetry of BAL quasars offer some of the best insights into the geometries of BAL outflows and tends to show a few key properties. The first is enhanced polarisation

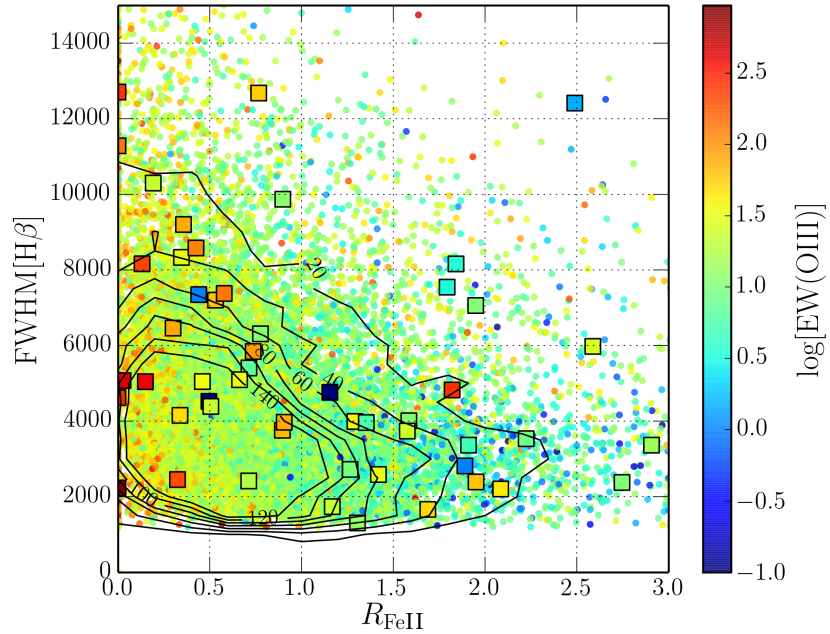


FIGURE 1.9: Eigenvector 1 for BAL and non-BAL quasars. FWHM of the H β line plotted against the relative iron strength, R_{FeII} . The colour coding corresponds to the EW of OIII. The dots mark all quasars from sample A, while the squares mark those with Mg II BALs. The triangles show the HST BAL quasars from sample B.

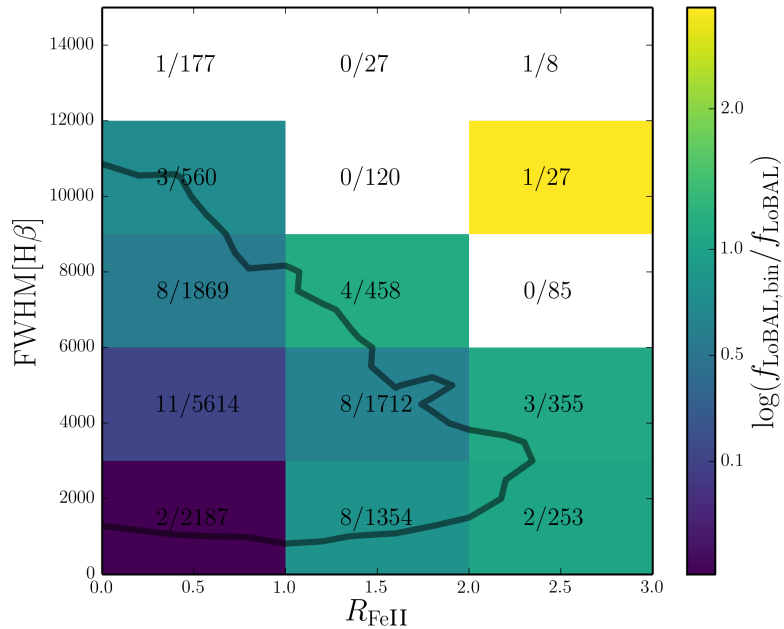


FIGURE 1.10: LoBAL fraction compared to global LoBAL fraction in Eigenvector 1 space, in bins of $\Delta R_{\text{FeII}} = 1$ and $\Delta \text{FWHM}[\text{H}\beta] = 3000 \text{ km s}^{-1}$. The contour shows the outermost contour from Fig. 1.9 for reference. The text shows $N_{\text{LoBAL}}/N_{\text{non-BAL}}$, where N_{LoBAL} is the number of LoBAL QSOs in the bin and $N_{\text{non-BAL}}$ in the number of non-BAL quasars in the bin.

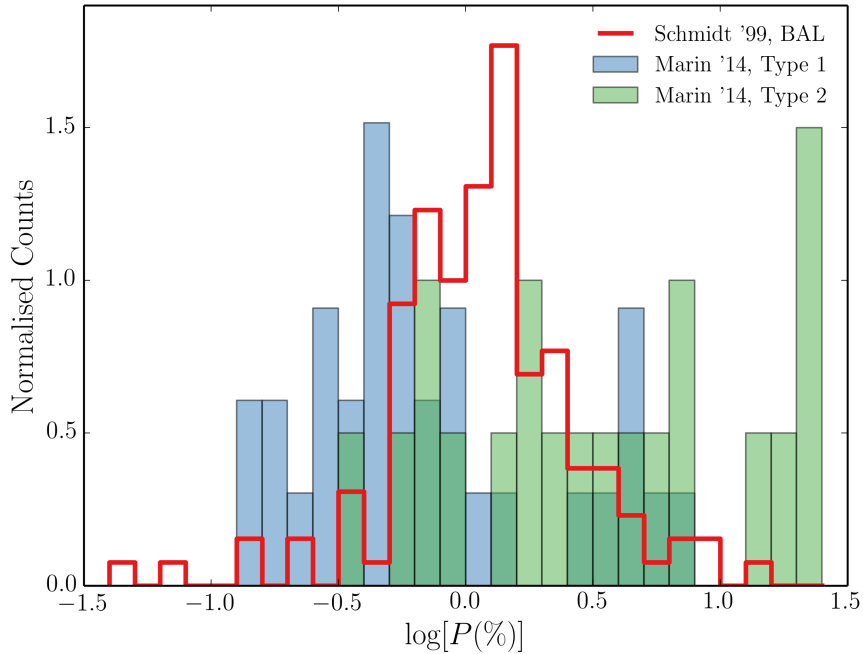


FIGURE 1.11: Histograms of polarisation percentages for BAL quasars from Schmidt et al. (1999) together with the Marin et al. (2014) AGN sample.

in the BAL troughs themselves (Schmidt & Hines 1999). This is readily explained by a scattering region unobscured by the BAL trough, with the higher polarisation percentage simply due to the decreased direct flux. This may also explain the non-black saturation in BAL troughs (see section ??).

The second property is a continuum polarisation percentage that is around 2.4 times greater, on average, than seen in the non-BAL population (Schmidt & Hines 1999). A histogram of the continuum polarisation percentages of a sample of BAL quasars from Schmidt & Hines (1999) are compared to the Type I and Type II AGN populations from Marin (2014) in Fig. 1.11. The corresponding cumulative distribution function is shown in Fig. 1.12. These show that BAL polarisation percentages seem to lie between those of type 1 and type 2 AGN. If type 1 and type 2 objects are viewed from low and high inclinations, respectively, as expected from unified models and suggested by Marin (2014, 2016), this would imply an intermediate inclination for BALQSOs. This enhanced polarisation for BALQSOs, relative to non-BAL systems, is also well reproduced by intermediate inclination outflows in simple radiative transfer models (Marin & Goosmann 2013).

The third characteristic polarisation property of BALQSOs is a polarisation angle of $\gtrsim 60^\circ$ with respect to the radio jet axis in RL objects (Brotherton et al. 2006, and

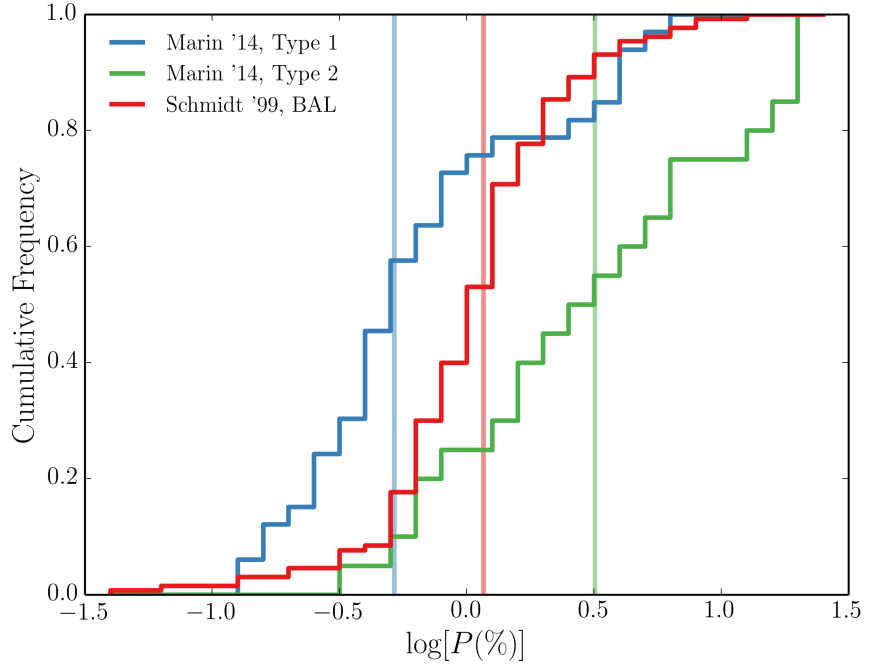


FIGURE 1.12: Cumulative distribution functions of the histograms shown in Fig. 1.11 for BAL quasars from Schmidt et al. (1999) together with the Marin et al. (2014) AGN sample. The colour-coding and x -axis scale are the same as Fig. 1.11. The translucent vertical lines mark the median value in each sample.

references therein). This suggests a higher inclination (compared to non-BAL quasars) viewing angle for BALQSOs under the interpretation of a geometric model. Indeed, early polarisation studies explained the observations with a polar scattering region, viewed at an equatorial angle (e.g. Goodrich & Miller 1995; Cohen et al. 1995; Lamy & Hutsemékers 2004). Regardless of the true geometry, the reason for the difference must be understood. I would suggest that polarisation predictions are made from wind models such as the one I presented in chapter 5, using a similar approach to Marin & Goosmann (2013), but considering BALs in more detail. Overall, however, polarisation measurements seem to imply that BALQSOs are viewed from higher inclinations if geometric unification models are correct and are in slight tension with the idea that BAL quasars are viewed from the same range of angles as non-BAL quasars.

1.5.3 The Effect of Obscuration

Caccianiga & Severgnini (2011, hereafter C11) showed that the distribution of $\text{EW}[\text{O III}]$ can also be well fitted by an obscuration model. They modelled the $\text{EW}[\text{O III}]$ distribution using an absorption model based on column densities obtained from the *XMM*

Newton Bright Serendipitous Source (XBS) sample. They use a sample size of 169 objects, and find that AGN with column densities of $N_H \gtrsim 10^{22} \text{ cm}^{-2}$ can explain the high EW powerlaw tail.

The column density measurements for BAL quasars suggest that obscuration cannot explain the distribution of EW[O III] in quasars. As briefly discussed in chapter 5, BALs generally show strong X-ray absorption with column densities of $N_H \gtrsim 10^{23} \text{ cm}^{-2}$ ([Green & Mathur 1996](#); [Mathur et al. 2000](#); [Green et al. 2001](#); [Grupe et al. 2003](#)). [Gallagher et al. \(1999\)](#) found all BAL quasars in a sample of 7 had $N_H > 10^{22} \text{ cm}^{-2}$, placing them firmly in the EW tail according to the C11 model. This is broadly consistent with the mean value of $3.5 \times 10^{22} \text{ cm}^{-2}$ from [Morabito et al. \(2013\)](#), and would imply that BALQSOs should have significantly higher EWs if obscuration governs the EW[O III] distribution. Of course, only LoBAL quasars had EW[O III] measurements in the sample used here – this actually strengthens the conclusion, as low ionization BALQSOs show even higher column densities, approaching Compton-thick values ([Morabito et al. 2011](#)). This holds regardless of the outflow geometry adopted, so I suggest that the obscured model of C11 is ruled out on this basis.

1.5.4 Line Anisotropy

Optically thin lines are isotropic – the *local* escape probabilities in each direction are equal due to the low optical depth. When lines are optically thick, the situation is more complex, as local velocity gradients then determine the line anisotropy. Indeed, Keplerian velocity shear has been shown to modify the shape of disc-formed emission lines ([Horne & Marsh 1986](#)), and an additional radial shear from a wind can cause double-peaked lines to become single-peaked ([Murray & Chiang 1996, 1997](#); [Flohic et al. 2012](#)).

R11 suggested that the broad emission lines trace the disc emission in terms of their anisotropy. If this was the case, we would not expect a difference in the BAL and non-BAL quasar EW distributions. However, an emission line would only be purely foreshortened if emitted by a disc with zero velocity shear. If the lines came from a region subject to Keplerian velocity shear then the surface brightness of an optically thick line is ([Horne & Marsh 1986](#))

$$J_{\text{thick}}(\theta) \approx \cos \theta \ S_L \ \Delta\nu \ \sqrt{8 \ln \tau_0}, \quad (1.4)$$

where S_L is the line source function and τ_0 is the line centre optical depth, given by

$$\tau_0 = \frac{\mathcal{W}}{\sqrt{2\pi\Delta\nu \cos\theta}}. \quad (1.5)$$

The parameter \mathcal{W} is given by

$$\mathcal{W} = \frac{\pi e^2}{m_e c} f N', \quad (1.6)$$

where f is the oscillator strength and N' is the number density integrated along the vertical height of the disc. The linewidth $\Delta\nu$ is enhanced from the thermal linewidth by the velocity shear, such that

$$\Delta\nu = \Delta\nu_{th} \left[1 + \left(\frac{3}{4} \frac{v_k}{v_{th}} \frac{H}{R} \right)^2 \sin^2\theta \tan^2\theta \sin^2 2\phi \right]^{1/2}. \quad (1.7)$$

Here, ϕ is the azimuthal angle in the disc, v_{th} and v_{th} are the thermal line width in frequency and velocity units respectively, H is the scale height of the disc at radius R , and v_k is the Keplerian velocity.

The outcome of the Horne & Marsh (1986) analysis is that optically thick lines formed in a Keplerian disc are strongly anisotropic, but they do not follow a simple $\cos\theta$ distribution. Instead, the angular emissivity function is a strong function of the velocity shear in the disc, the atomic physics of the line in question, the location of the line formation region and the vertical disc structure. It is hence possible that the broad emission lines are strongly anisotropic, and the presence of radial velocity shear from a wind would only complicate matters. I would therefore suggest that future efforts might include fully modelling the line emission as a function of inclination to feed into the above analysis.

Regardless of the precise angular distribution, line emission should not trace disc emission exactly, as we already know large-scale velocity fields are dynamically important in the BLR, purely from the line widths. In that case, one would expect systematic differences in EW between high inclination and low inclination sources, and these are not seen in the C IV 1550 Å and Mg II 2800 Å EW distributions.

1.6 Conclusions

I have explored the emission line properties of BAL and non-BAL quasars, particularly focusing on the EW distributions in two redshift ranges of the SDSS quasar catalog.

My main conclusion is simply that the EW distributions of BAL and non-BAL quasars are remarkably similar, and this is not what one would expect from a unification model in which an equatorial BAL outflow rises from a foreshortened accretion disc. This geometry has been used extensively in geometric unification and BAL outflow models in the past (e.g. Murray et al. 1995; Proga et al. 2000; Proga & Kallman 2004; Risaliti & Elvis 2010; Borguet & Hutsemékers 2010; Higginbottom et al. 2013; Nomura et al. 2013, 2016), and was even adopted earlier in this thesis. I then established that an angular emissivity function of $\epsilon(\theta) = \cos \theta$ is actually the conservative estimate from thin disc models, and used this to conduct a series of simulations similar to those conducted by Risaliti et al. (2011). As expected, these simulations confirmed the above finding.

Based on this analysis, it is possible to construct a few possible scenarios that favoured by the above results. These conclusions have the caveat that I have assumed that conclusions drawn about LoBAL quasars can be extended to BAL quasars in general.

- **Scenario 1:** The quasar continuum is much more isotropic than one would expect from a geometrically thin, optically thick accretion disc. I have demonstrated that general relativistic effects cannot account for this discrepancy in the UV. Reprocessing by surrounding dense plasma with a large covering factor or limb brightening in the disc may provide possible explanations which this analysis cannot yet confirm or refute.
- **Scenario 2:** Quasar discs are strongly anisotropic, as expected from a geometrically thin, optically thick accretion disc. In this case, BAL outflows cannot only emerge at extreme inclinations and should instead be seen at very similar angles to non-BAL quasars. Polarisation measurements need to be reconciled with this hypothesis. I recommend that future RT modelling efforts explore different outflow geometries and that detailed polarisation modelling is undertaken to constrain the outflow opening angles.
- **Scenario 3:** The geometric unification model does not explain the incidence of BALs in quasars, or requires an additional component which is *time-dependent*, such as an evolutionary or accretion state origin for BAL outflows. In this scenario, BAL quasars would be seen from very similar angles to non-BAL quasars. If this is the case, the covering factors and opening angles of the outflows still need to be constrained so that feedback efficiencies can be accurately estimated.

I have confirmed that obscuration cannot explain the EW distributions of all quasars due to the high column density observed in BAL (and particularly LoBAL) quasars. It is possible that line opacity could explain the observed similarities between the broad emission line distributions, but this cannot explain the similarities in the LoBAL and non-BAL quasar EW[O III] distributions, as O III is a forbidden, optically thin transition.

Regardless of the conclusions about BAL quasars and their outflow geometries, this analysis allows conclusions to be drawn about the *overall* quasar population. In scenario 1, the EW[O III] distribution of quasars cannot be driven by inclination as suggested by ([Risaliti et al. 2011](#)). This would imply that EW[O III] is a poor orientation indicator. The lack of correlation between EW[O III] and FWHM[H β] also suggests that it is not possible for them both to be strongly orientation dependent. Even if scenario 1 holds, then FWHM[H β] and EV1 measurements of LoBALS imply that they are seen from similar inclinations to type 1 quasars.

The above three scenarios each pose a different challenge to the current understanding of, respectively, accretion physics, outflow models and our understanding of unification and the BAL fraction. This work therefore adds to the growing evidence that our simplest models are not sufficient to describe the overall quasars and that alternatives should be sought.

Bibliography

- Borguet B., Hutsemékers D., 2010, A&A 515, A22
- Borguet B. C. J., Edmonds D., Arav N., Dunn J., Kriss G. A., 2012, ApJ 751, 107
- Boroson T. A., Green R. F., 1992, ApJs 80, 109
- Brotherton M. S., De Breuck C., Schaefer J. J., 2006, MNRAS 372, L58
- Caccianiga A., Severgnini P., 2011, MNRAS 415, 1928
- Capellupo D. M., Netzer H., Lira P., Trakhtenbrot B., Mejía-Restrepo J., 2015, MNRAS 446, 3427
- Cohen M. H., Ogle P. M., Tran H. D., Vermeulen R. C. et al., 1995, ApJ Letters 448, L77
- Dai X., Shankar F., Sivakoff G. R., 2012, ApJ 757, 180
- Davis S. W., Hubeny I., 2006, ApJs 164, 530
- Davis S. W., Woo J.-H., Blaes O. M., 2007, ApJ 668, 682
- DiPompeo M. A., Brotherton M. S., Cales S. L., Runnoe J. C., 2012a, MNRAS 427, 1135
- DiPompeo M. A., Brotherton M. S., De Breuck C., 2012b, ApJ 752, 6
- Flohic H. M. L. G., Eracleous M., Bogdanović T., 2012, ApJ 753, 133
- Gallagher S. C., Brandt W. N., Sambruna R. M., Mathur S., Yamasaki N., 1999, ApJ 519, 549
- Goodrich R. W., Miller J. S., 1995, ApJ Letters 448, L73
- Green P. J., Aldcroft T. L., Mathur S., Wilkes B. J., Elvis M., 2001, ApJ 558, 109
- Green P. J., Mathur S., 1996, ApJ 462, 637
- Grupe D., Mathur S., Elvis M., 2003, AJ 126, 1159
- Higginbottom N., Knigge C., Long K. S., Sim S. A., Matthews J. H., 2013, MNRAS 436, 1390
- Horne K., Marsh T. R., 1986, MNRAS 218, 761
- Hubeny I., Agol E., Blaes O., Krolik J. H., 2000, ApJ 533, 710

- Lamy H., Hutsemékers D., 2004, A&A 427, 107
- Lazarova M. S., Canalizo G., Lacy M., Sajina A., 2012, ApJ 755, 29
- Long K. S., Knigge C., 2002, ApJ 579, 725
- Marin F., 2014, MNRAS 441, 551
- Marin F., 2016, ArXiv e-prints
- Marin F., Goosmann R. W., 2013, MNRAS 436, 2522
- Marziani P., Sulentic J. W., Zwitter T., Dultzin-Hacyan D., Calvani M., 2001, ApJ 558, 553
- Mathur S., Green P. J., Arav N., Brotherton M. et al., 2000, ApJ Letters 533, L79
- Mihalas D., 1978, Stellar atmospheres /2nd edition/
- Morabito L. K., Dai X., Leighly K. M., Sivakoff G. R., Shankar F., 2011, ApJ 737, 46
- Morabito L. K., Dai X., Leighly K. M., Sivakoff G. R., Shankar F., 2013, ArXiv e-prints
- Muñoz-Darias T., Coriat M., Plant D. S., Ponti G. et al., 2013, MNRAS 432, 1330
- Murray N., Chiang J., 1996, Nature 382, 789
- Murray N., Chiang J., 1997, ApJ 474, 91
- Murray N., Chiang J., Grossman S. A., Voit G. M., 1995, ApJ 451, 498
- Nomura M., Ohsuga K., Takahashi H. R., Wada K., Yoshida T., 2016, PASJ 68, 16
- Nomura M., Ohsuga K., Wada K., Susa H., Misawa T., 2013, PASJ 65, 40
- Proga D., 2005, in J.-M. Hameury, J.-P. Lasota (eds.), *The Astrophysics of Cataclysmic Variables and Related Objects*, Vol. 330 of *Astronomical Society of the Pacific Conference Series*, 103
- Proga D., Kallman T. R., 2004, ApJ 616, 688
- Proga D., Stone J. M., Kallman T. R., 2000, ApJ 543, 686
- Risaliti G., Elvis M., 2010, A&A 516, A89
- Risaliti G., Salvati M., Marconi A., 2011, MNRAS 411, 2223
- Schmidt G. D., Hines D. C., 1999, ApJ 512, 125
- Shen Y., Ho L. C., 2014, Nature 513, 210
- Shen Y., Richards G. T., Strauss M. A., Hall P. B. et al., 2011, ApJs 194, 45
- Sim S. A., Drew J. E., Long K. S., 2005, MNRAS 363, 615
- Sulentic J. W., Zwitter T., Marziani P., Dultzin-Hacyan D., 2000, ApJ Letters 536, L5
- Urrutia T., Becker R. H., White R. L., Glikman E. et al., 2009, ApJ 698, 1095
- Vestergaard M., Wilkes B. J., 2001, ApJs 134, 1
- Weymann R. J., Morris S. L., Foltz C. B., Hewett P. C., 1991, ApJ 373, 23
- Zhang S. N., Cui W., Chen W., 1997, ApJ Letters 482, L155

Zhou H., Wang T., Wang H., Wang J. et al., 2006, ApJ 639, 716